Computational Insights Into the Electronic Structure and Magnetic Properties of Rhombohedral Type Half-Metal GdMnO$_3$ With Multiple Dirac-Like Band Crossings

Yu Chang [1,2], Sung-Ryong Moon [2*], Xin Wang [1,2*], Rabah Khenata [3*], H. Khachai [4] and Minquan Kuang [5*]

[1] Tonghua Normal University, Tonghua, China, [2] Department of Electronic Engineering, Wonkwang University, Iksan, South Korea, [3] Laboratoire de Physique Quantique de La Matiere et de Modelisation Mathematique (LPQ3M), Université de Mascara, Mascara, Algeria, [4] Laboratoire D'etude des Materiaux & Instrumentations Optiques, Physics Department, Djillali Liabès University of Sidi Bel-Abbès, Sidi Bel Abbès, Algeria, [5] School of Physical Science and Technology, Southwest University, Chongqing, China

In spintronics, half-metallic materials (HMMs) with Dirac-like cones exhibit interesting physical properties such as massless Dirac fermions and full spin polarization. We combined first-principles calculations with the quasi-harmonic Debye model, and we proposed that the rhombohedral GdMnO$_3$ is an HMM with multiple linear band crossings. The physical properties of GdMnO$_3$ were studied thoroughly. Moreover, the changes of multiple linear band crossings and 100% spin polarization under spin-orbit coupling as well as the electron and hole doping were also investigated. It is noted that such spin-polarized HMMs with linear band crossings are still very rare in two-dimensional and three-dimensional materials.

Keywords: half-metal, spintronics, DFT, electronic structures, rhombohedral, spin-polarization

Different from traditional electronics, spintronics mainly use spin rather than charge as a carrier for transmitting and processing information (Awschalom and Flatté, 2007), greatly improving the performance and effectively reducing the power consumption of electronic devices. The field of spintronics has developed rapidly in recent years, but it still faces many challenges, such as long distance spin transport, spin-polarized carrier generation and injection, and spin manipulation and detection. In response to these problems, scientists have proposed a series of spintronic materials such as spin gapless semiconductors (SGS) (Wang, 2008, 2017; Wang et al., 2010, 2016, 2017, 2018; Han et al., 2018), zero-gap half-metals (HMs) (Du et al., 2013), Dirac HMs (Ishizuka and Motome, 2012; He et al., 2016; Liu et al., 2017; Zhang et al., 2017), dilute magnetic semiconductors (DMS) (Furdyna, 1988), and bipolar Magnetic Semiconductor (BMS) (Li et al., 2012).

Currently, the new generation of spintronics also faces a problem of achieving zero-energy consumption and ultra-high speed for electronic transmission. Dirac-type half-metallic materials are excellent candidates for achieving these goals because they have the advantages of having massless Dirac fermions and high spin polarization. The first Dirac half-metal (DHMs) was theoretically verified in triangular ferromagnet (Ishizuka and Motome, 2012). Since then, research on DHMs has mainly focused on two-dimensional materials (He et al., 2016; Liu et al., 2017). Very recently, a three-dimensional material, MnF$_3$ with multiple Dirac cones near the Fermi level was predicted by Jiao et al. (2017). Compared to the materials with a single-Dirac-cone DHM, materials with multiple Dirac band dispersions can exhibit higher carrier transmission efficiency and stronger

FIGURE 1 | (Left) Crystal structures of the $R\bar{3}c$-type GdMnO₃ material with hexagonal structure; (Right) four magnetic structures, i.e., FM, NM, and two AFM structures (labeled as AFM-1, and AFM-2).

FIGURE 2 | Spin-density of GdMnO₃ obtained by the DFT+U method.
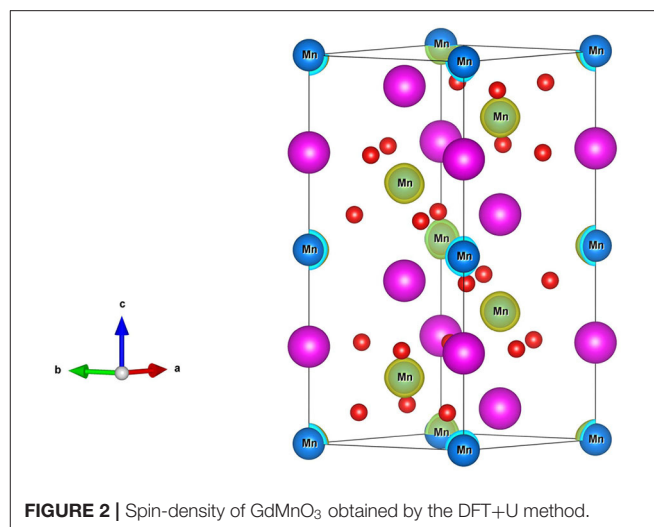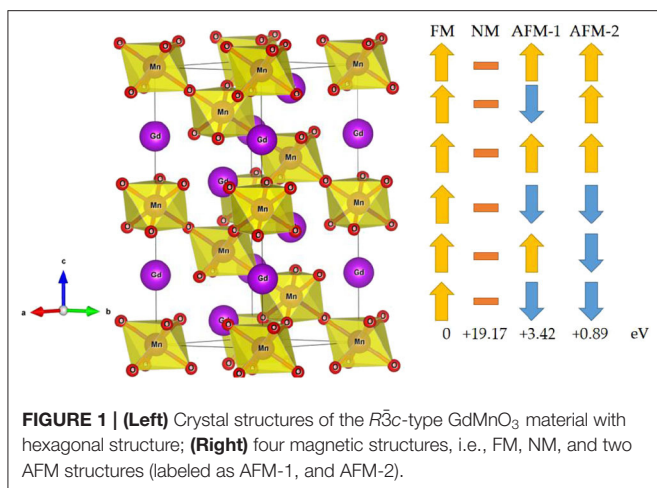
non-linear electromagnetic response. Subsequently, LaMnO₃ (Ma et al., 2018) with the $R\bar{3}c$ type structure was proposed by Du's group in 2018 to display complete spin-polarization and multiple Dirac cones around the Fermi level.

Unfortunately, the types and number of DHMs is extremely limited. Therefore, it is necessary to design more HMMs with Dirac-like band crossings and 100% spin polarization. In this work, we will study the electronic structures, magnetism, and thermodynamic properties of the $R\bar{3}c$ type GdMnO₃ using first-principles calculations incorporating the quasi-harmonic Debye model (QDM). Furthermore, the spin-orbit coupling, and the electron and hole doping effects were taken into consideration to examine the stability of the electronic structure. A more detailed description of the Computational Methods is provided in the **Supplementary Information**.

The $R\bar{3}c$-type GdMnO₃ crystal structure with hexagonal setting is shown in **Figure 1** (Left). The GdMnO₃ crystal structure belongs to space group number 167 and the optimized equilibrium lattice parameters for the FM state are a = b = 5.63 Å and c = 13.17 Å. The six Mn atoms have four types of magnetic orderings, namely, FM, NM, AFM-1, and AFM-2. As shown in **Figure 1** (Right), the spin orderings of the six Mn are ↑↑↑↑↑↑, ↑↓↑↓↑↓, and ↑↑↑↑↓↓ respectively, for FM, AFM-1 and AFM-2 configurations. By fully relaxing the crystal structures of GdMnO₃ and checking the magnetic structures of this GdMnO₃. From **Figure 1** (Right), one can conclude that the most stable magnetic phase is the FM phase due to its lowest total energy. The calculated total magnetic moment of this material under FM and equilibrium lattice constant is 24 μ_B per unit cell, and arises mainly from the Mn atoms (the spin density of GdMnO₃ is given in **Figure 2**), with the atomic magnetic moment of each Mn atom of ~4.4 μ_B.
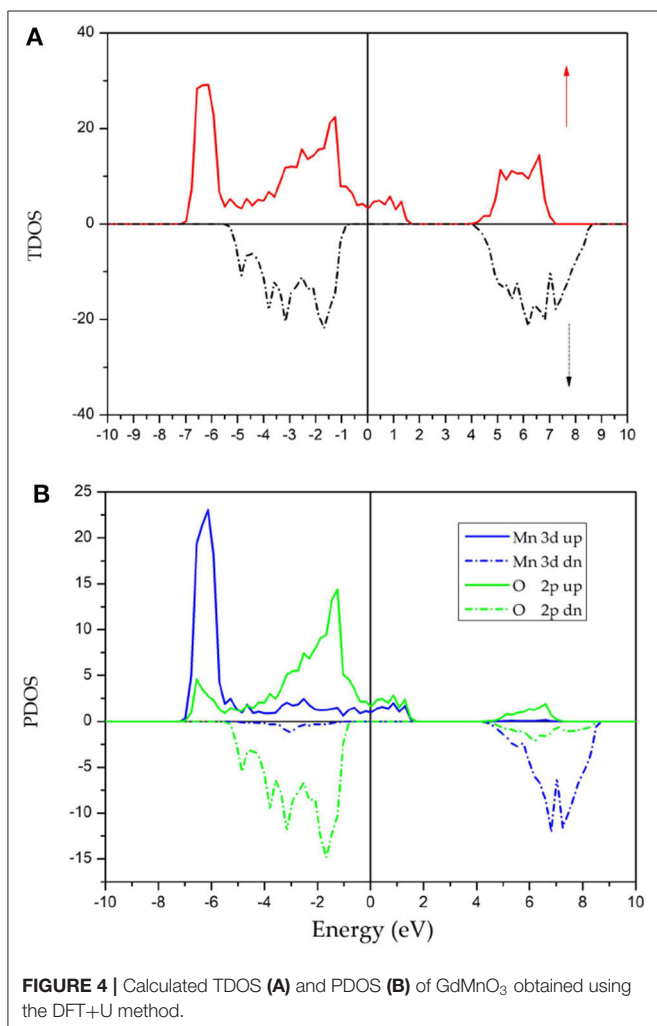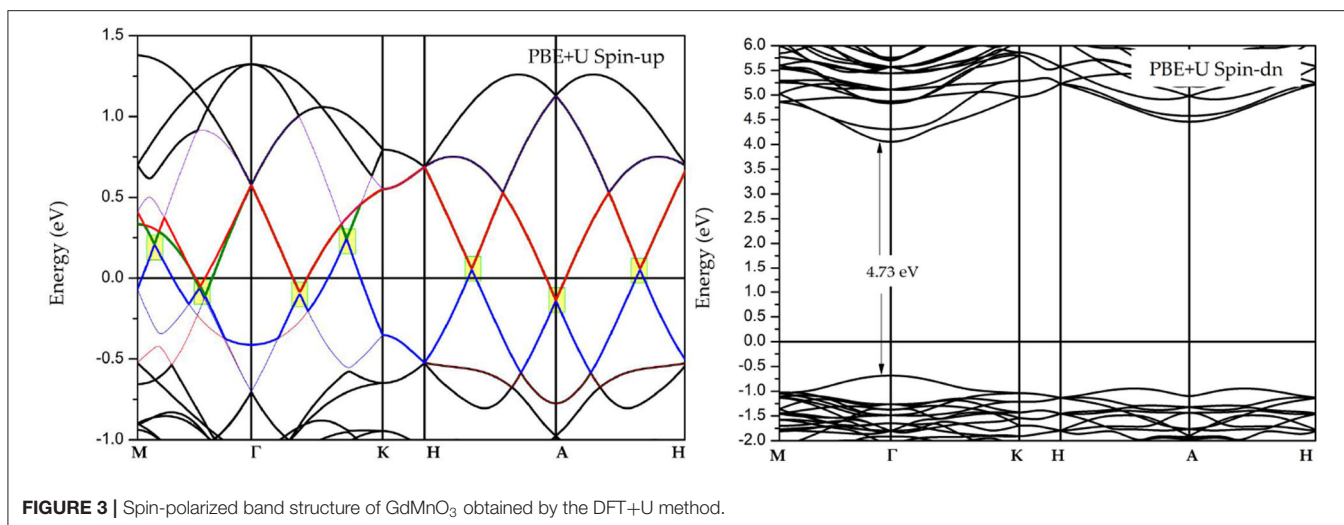
Figure 3 shows the spin-polarized band structures of GdMnO₃ obtained by DFT+U calculations. To accurately describe the electronic structures of GdMnO₃, the on-site Coulomb interaction U and exchange interaction J were set to 10.1 and 0.88 eV, respectively, for Mn-3d based on reference (Ma et al., 2018). An examination of the band structure shows that while the band gap (~4.73 eV) and the half-metallic band

gap (~0.75 eV) is found in the spin-down channel, the bands in the spin-up channel show metallic properties, suggesting that GdMnO₃ is a half-metallic material (Anjami et al., 2017; Jiao et al., 2017; Ma et al., 2018). Normally, a large energy gap (difference between the energies of the highest occupied and lowest unoccupied in the spin-down channel) and a half-metallic band gap (difference between the energies of highest occupied and the Fermi level in the spin-down channel) are considered to be evidence of robust half-metallic behaviors.
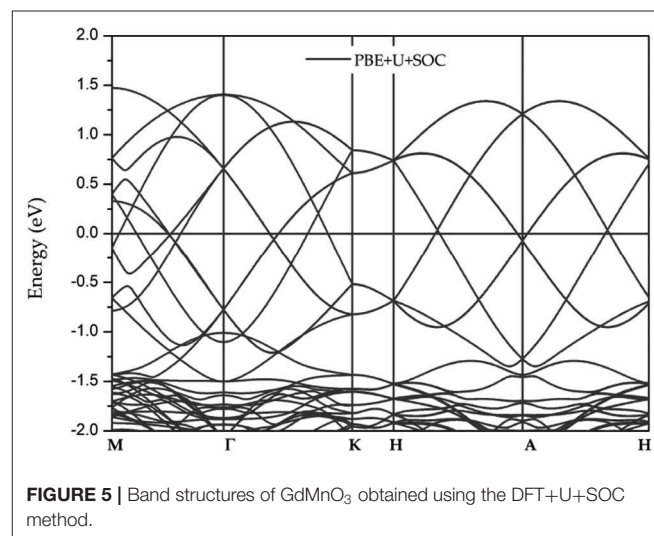
Interestingly, in the spin-up channel, there are some Dirac-like band crossings that are very close to the Fermi level. In **Figure 3**, we used yellow squares to highlight the regions of the Dirac-like crossing points near the Fermi level. Clearly, three Dirac-like crossing points are present along the M–Γ path, two Dirac-like crossing points are present along the Γ-K path, one Dirac-like crossing point is located at the A high symmetry point, and a Dirac-like crossing point is found along the A–H path.

Figure 4 shows the TDOS and PDOS of GdMnO₃ in both spin directions obtained using the DFT+U method. Spin polarization (%) is a highly important parameter and can be expressed as Jiao et al. (2017): $P = \frac{|N\uparrow(E_f) - N\downarrow(E_f)|}{|N\uparrow(E_f) + N\downarrow(E_f)|} \times 100$ where $N\uparrow(E_f)$ and $N\downarrow(E_f)$. Here, $N\uparrow(E_f)$ is the number of the spin-up states and $N\uparrow(E_f)$ is the number of the spin-down states. An examination of **Figure 4A** shows that the P-value of GdMnO₃ is 100%, indicating that GdMnO₃ can be selected for using in future spintronic devices.

An examination of **Figure 4B** shows a clear energy gap in the vicinity of the Fermi level in the spin-down channel; however, the spin-up electrons show metallic behavior. For the spin-up channel, the density of states primarily arises from the d states of the Mn atoms and the p states of O atoms. It is important to note that the DOS peak at approximately −7 eV (7 eV) of the spin-down channel (spin-up channel) is induced due to the strong spin splitting (Qin et al., 2017; Han et al., 2019) of the Mn atoms. At the same time, the nearly symmetrical DOS of O in both spin directions suggest that the atomic magnetic moments of O can be ignored.
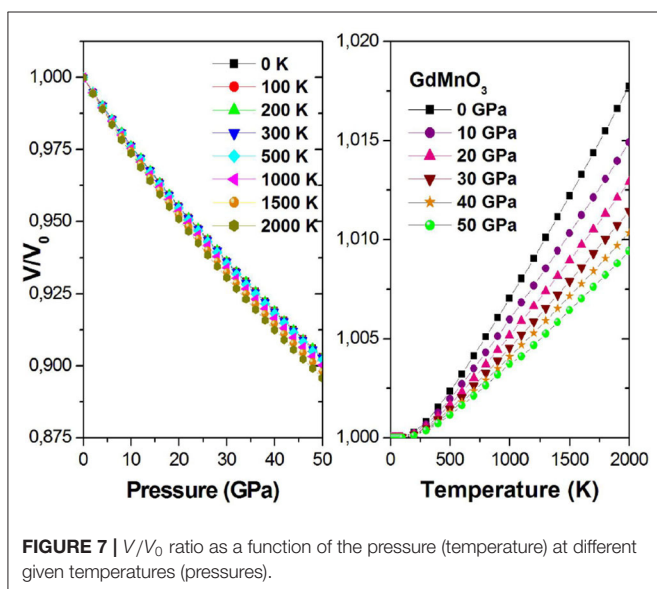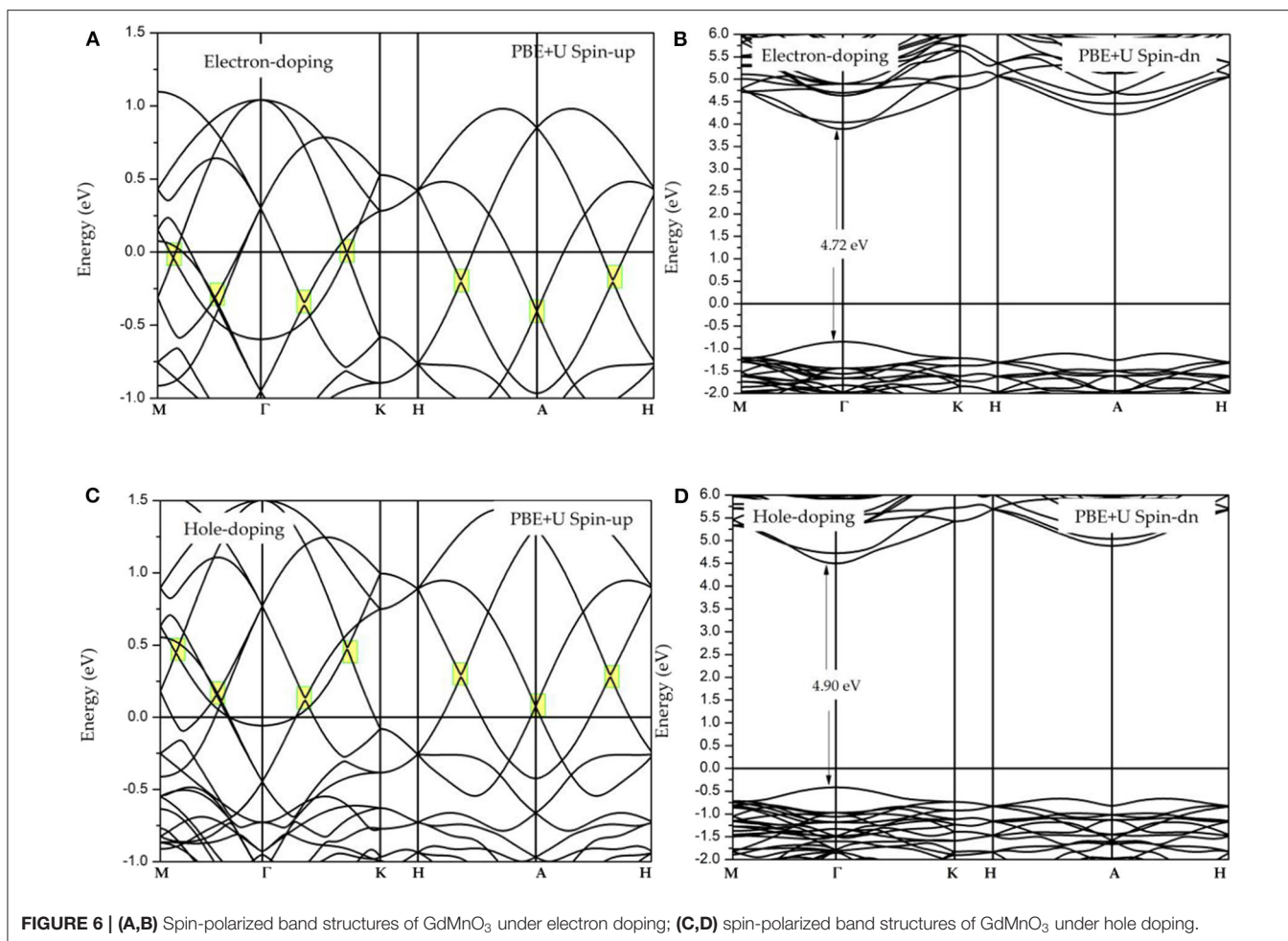
FIGURE 3 | Spin-polarized band structure of GdMnO$_3$ obtained by the DFT+U method.

FIGURE 4 | Calculated TDOS (A) and PDOS (B) of GdMnO$_3$ obtained using the DFT+U method.

FIGURE 5 | Band structures of GdMnO$_3$ obtained using the DFT+U+SOC method.

by DFT+U+SOC calculations. It is observed that the Dirac-like band crossings is still present when the SOC is taken into account, namely, the conduction and valence bands are still degenerate. Due to the robustness with respect to the SOC effect, GdMnO$_3$ features long spin coherence which is helpful for spintronic applications.

It is well-known that electron and hole doping may influence the stability of the electronic structure around the Fermi level. Therefore, in this work, we will study the effect of electron and hole doping on the band structure. The doping concentration of each atom is 0.025 carrier, and the obtained band structures under the electron doping and under hole doping are shown in **Figures 6A–D**, respectively. An examination of these figures shows that electron doping will increase the energy of the Fermi level, while hole doping will decrease the Fermi level energy. Both electron and hole doping have no obvious effect on the Dirac-like band crossings and half-metallic states (see **Figures 6A,C**) with the exception of changing the location of the Dirac-like band

Because the GdMnO$_3$ system contains heavy atoms, the effect of the spin-orbit coupling (SOC) should be discussed in this work. **Figure 5** shows the band structures of GdMnO$_3$ obtained

FIGURE 6 | (A,B) Spin-polarized band structures of GdMnO₃ under electron doping; **(C,D)** spin-polarized band structures of GdMnO₃ under hole doping.

FIGURE 7 | V/V_0 ratio as a function of the pressure (temperature) at different given temperatures (pressures).
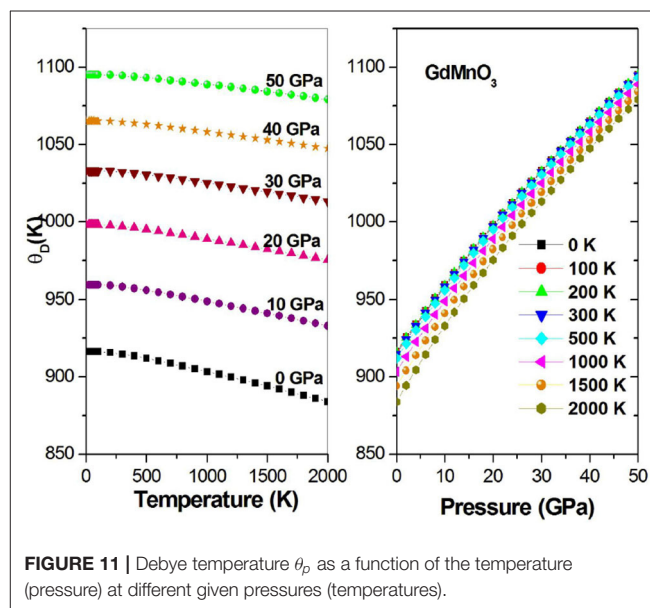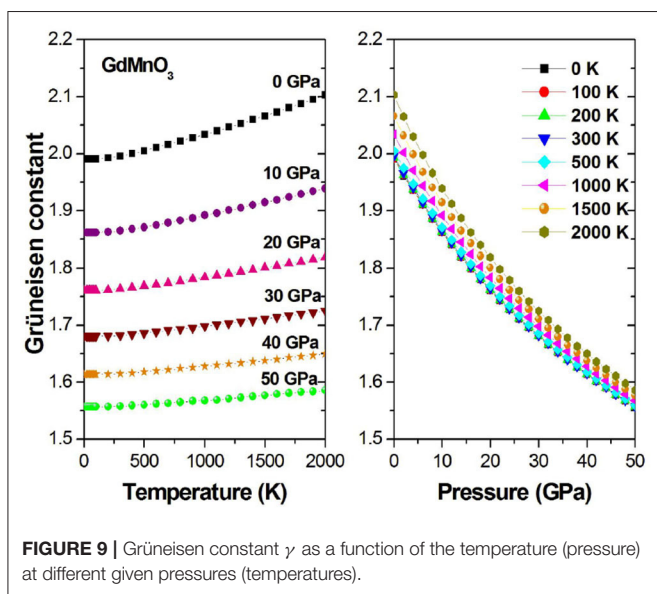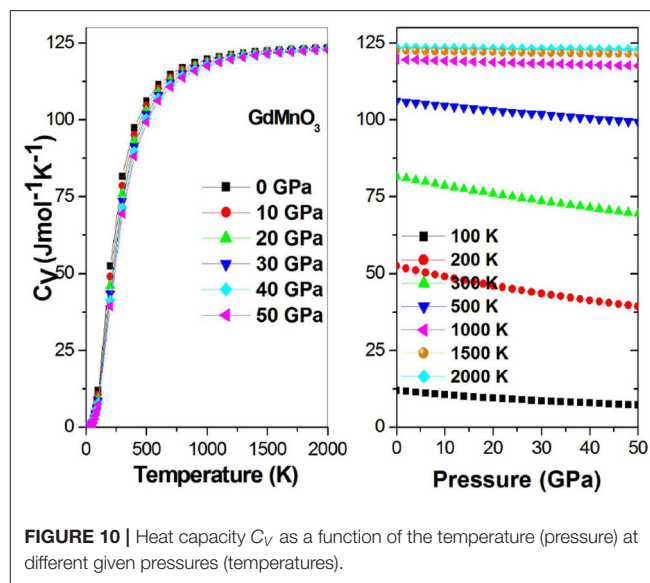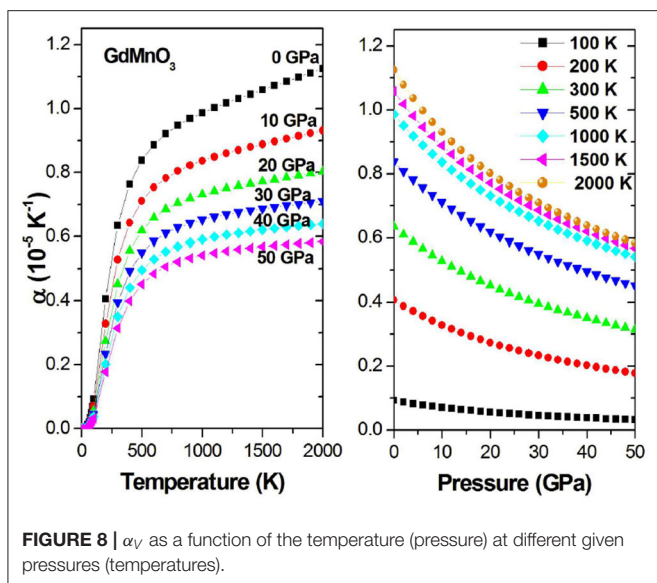
crossing points. The carrier concentration, can be adjusted by use of a gate voltage (Thelander et al., 2004).

Then, we calculated some thermodynamic parameters to understand the thermodynamic behavior of GdMnO₃ under high temperature and high pressure limits. As mentioned in the Computational method section, in this work, QDM is used to investigate the thermodynamic properties, and the investigated temperature and pressure regions were 0–2,000 K and 0–50 GPa, respectively.

Figure 7 shows the relationship between the V/V_0 rate of change and temperature and pressure, where V_0 is the initial volume and V is the final volume for a given pressure. In **Figure 7** (Left), we can clearly find that for a given fixed temperature, the rate V/V_0 decreases with increasing pressure. This is a negative correlation; in other words, the slope is negative. As observed from **Figure 7** (Right), the V/V_0 rate and temperature are positively correlated.

The relationships between α_V on the one hand and pressure and temperature on the other hand are shown in **Figure 8**. For a fixed pressure, with increasing temperature, α_V increases first sharply and then slowly. This may be due to the higher pressure limiting the rise of α_V. **Figure 8** (Right) shows that for a constant temperature, although the increase in the pressure will gradually decrease α_V, for higher temperature, the increase in the

FIGURE 8 | α_V as a function of the temperature (pressure) at different given pressures (temperatures).

FIGURE 10 | Heat capacity C_V as a function of the temperature (pressure) at different given pressures (temperatures).

FIGURE 9 | Grüneisen constant γ as a function of the temperature (pressure) at different given pressures (temperatures).

FIGURE 11 | Debye temperature θ_p as a function of the temperature (pressure) at different given pressures (temperatures).

pressure will only increase the initial value of α_V without affecting the trend.

Using the Grüneisen parameter (γ) to predict the thermodynamic properties of the material at high temperatures and pressures, we can evaluate the effect of the crystal anharmonicity. **Figure 9** shows the relationship between γ on the one hand and the pressure and temperature on the other hand, and it is observed that with increasing temperature or decreasing pressure, the pressure/temperature relationship increases accordingly.

Figure 10 shows that the heat capacity of GdMnO$_3$ shows a close to cubic dependence on the temperature (T^3) at low temperatures, suggesting that lattice vibrations will increase with increasing temperature. Moreover, the high temperature value is

constant, as stated by the Dulong-Petti limit, indicating that the thermal energy at high temperature excites all phonon modes. The increase in the absolute pressure increase is a negative effect and will stop lattice vibrations.

Figure 11 shows the Debye temperature and its relation to the temperature at fixed pressures and the Debye temperature and its relationship to the pressure at fixed temperatures. The value of θ_p has a negative quasi-linear relationship with temperature and a positive quasi-linear relationship with pressure.

In this study, a new material, perovskite $R\bar{3}c$ type GdMnO$_3$, with half-metallic behavior and multiple linear band crossing was examined and its electronic, magnetic, and thermodynamic properties were investigated via first-principles and QDM calculations. In this work, different magnetic structures were considered, namely, FM, NM, AFM-1, and AFM-2. We found

that FM is the most stable due to its lowest total energy. The SOC effect has a weak effect on the electronic structure and therefore this material may have the potential for long spin coherence for long-range spin transport. The effects of electron and hole doping were also included in this calculation. We found the properties of half-metallicity and multiple linear band crossings are highly robust against electron and hole doping.

DATA AVAILABILITY STATEMENT

The raw data supporting the conclusions of this article will be made available by the authors, without undue reservation.

AUTHOR CONTRIBUTIONS

YC: software, methodology, and writing. S-RM: supervisor. XW, RK, and HK: reviewing and editing. MK: conceptualization. All authors contributed to the article and approved the submitted version.

SUPPLEMENTARY MATERIAL

REFERENCES

Anjami, A., Boochani, A., Elahi, S. M., and Akbari, H. (2017). Ab-initio study of mechanical, half-metallic and optical properties of Mn_2ZrX (X= Ge, Si) compounds. *Results Phys.* 7, 3522–3529. doi: 10.1016/j.rinp.2017.09.008

Awschalom, D. D., and Flatté, M. E. (2007). Challenges for semiconductor spintronics. *Nat. phys.* 3, 153–159. doi: 10.1038/nphys551

Du, Y., Xu, G. Z., Zhang, X. M., Liu, Z., Yu, S., Liu, E., et al. (2013). Crossover of magnetoresistance in the zero-gap half-metallic Heusler alloy Fe_2CoSi. *EPL* 103:37011. doi: 10.1209/0295-5075/103/37011

Furdyna, J. K. (1988). Diluted magnetic semiconductors. *J. Appl. Phys.* 64, R29–R64. doi: 10.1063/1.341700

Han, Y., Chen, Z., Kuang, M., Liu, Z., Wang, X., and Wang, X. (2019). 171 Scandium-based full Heusler compounds: A comprehensive study of competition between XA and $L2_1$ atomic ordering. *Results Phys.* 12, 435–446. doi: 10.1016/j.rinp.2018.11.079

Han, Y., Khenata, R., Li, T., Wang, L., and Wang, X. (2018). Search for a new member of parabolic-like spin-gapless semiconductors: the case of diamond-like quaternary compound $CuMn_2InSe_4$. *Results Phys.* 10, 301–303. doi: 10.1016/j.rinp.2018.06.031

He, J., Ma, S., Lyu, P., and Nachtigall, P. (2016). Unusual Dirac half-metallicity with intrinsic ferromagnetism in vanadium trihalide monolayers. *J. Mater. Chem. C.* 4, 2518–2526. doi: 10.1039/C6TC00409A

Ishizuka, H., and Motome, Y. (2012). Dirac half-metal in a triangular ferrimagnet. *Phys. Rev. Lett.* 109:237207. doi: 10.1103/PhysRevLett.109.237207

Jiao, Y., Ma, F., Zhang, C., Bell, J., Sanvito, S., and Du, A. (2017). First-principles prediction of spin-polarized multiple Dirac rings in manganese fluoride. *Phys. Rev. Lett.* 119:016403. doi: 10.1103/PhysRevLett.119.016403

Li, X., Wu, X., Li, Z., Yang, J., and Hou, J. G. (2012). Bipolar magnetic semiconductors: a new class of spintronics materials. *Nanoscale* 4, 5680–5685. doi: 10.1039/c2nr31743e

Liu, Z., Liu, J., and Zhao, J. (2017). YN_2 monolayer: novel p-state Dirac half metal for high-speed spintronics. *Nano Res.* 10, 1972–1979. doi: 10.1007/s12274-016-1384-3

Ma, F., Jiao, Y., Jiang, Z., and Du, A. (2018). Rhombohedral lanthanum manganite: a new class of dirac half-metal with promising potential in spintronics. *ACS Appl. Mater. Interfaces* 10, 36088–36093. doi: 10.1021/acsami.8b09349

Qin, G., Wu, W., Hu, S., Tao, Y., Yan, X., Jing, C., et al. (2017). Effect of swap disorder on the physical properties of the quaternary heusler alloy PdMnTiAl: a first-principles study. *IUCrJ* 4, 506–511. doi: 10.1107/S205225251700745X

Thelander, C., Bjork, M. T., Larsson, M. W., Hansen, A. E., Wallenberg, L. R., and Samuelson, L. (2004). Electron transport in InAs nanowires and heterostructure nonowire devices. *Solid State Commun.* 131:573. doi: 10.1016/j.ssc.2004.05.033

Wang, X., Cheng, Z., Liu, G., Dai, X., Khenata, R., Wang, L., et al. (2017). Rare earth-based quaternary Heusler compounds MCoVZ (M= Lu, Y; Z= Si, Ge) with tunable band characteristics for potential spintronic applications. *IUCrJ* 4, 758–768. doi: 10.1107/S2052252517013264

Wang, X., Cheng, Z., Wang, J., Wang, X.-L., and Liu, G. D. (2016). Recent advances in the Heusler based spin-gapless semiconductors. *J. Mater. Chem. C.* 4, 7176–7192. doi: 10.1039/C6TC01343K

Wang, X., Li, T., Cheng, Z., Wang, X.-L., and Chen, H. (2018). Recent advances in Dirac spin-gapless semiconductors. *Appl. Phys. Rev.* 5:041103. doi: 10.1063/1.5042604

Wang, X. L. (2008). Proposal for a new class of materials: spin gapless semiconductors. *Phys. Rev. Lett.* 100:156404. doi: 10.1103/PhysRevLett.100.156404

Wang, X. L. (2017). Dirac spin-gapless semiconductors: promising platforms for massless and dissipationless spintronics and new (quantum) anomalous spin Hall effects. *Natl. Sci. Rev.* 4, 252–257. doi: 10.1093/nsr/nww069

Wang, X. L., Dou, S. X., and Zhang, C. (2010). Zero-gap materials for future spintronics, electronics and optics. *NPG Asia Mater.* 2, 31–38. doi: 10.1038/asiamat.2010.7

Zhang, S., Zhang, C., Zhang, S., Ji, W., Li, P., Wang, P., et al. (2017). Intrinsic Dirac half-metal and quantum anomalous Hall phase in a hexagonal metal-oxide lattice. *Phys. Rev. B.* 96:205433. doi: 10.1103/PhysRevB.96.205433